[Article ID] 1003- 6326(2001)06- 0838- 05

Wear resistance and hot corrosion behaviour of laser cladding Co-based alloy①

ZHANG Song(张 松)[1,2], ZHANG Chun-hua(张春华)[1], MAN Hau-chung(文效忠)[3], WU Wei-tao(吴维岧)[2], WANG Mao-cai(王茂才)[2]

(1. School of Materials Science and Engineering, Shenyang Polytechnic University, Shenyang 110023, P. R. China;
2. State Key Laboratory for Corrosion and Protection of Metals, Chinese Academy of Science, Shenyang 110016, P. R. China;
3. Department of Manufacturing Engineering, Hong Kong Polytechnic University, Hong Kong, P. R. China)

[Abstract] 2Cr13 stainless steel was surface cladded with Co-based alloy using a high power carbon dioxide laser. The microstructure, wear resistance and corrosion properties of the clad layer were investigated. It is found that the high temperature corrosion behavior and wearing resistant property of the clad layer are 3 and 2.5 times higher than those of the parent metal. Under the high temperature molten lead sulphate salt corrosion condition, the clad layer fails by spalling which is caused by intergrannular corrosion within the clad layer. The fine dendritic structure and the oxide help to retard the penetration of the sulphur ion that induces the intergrannular corrosion.

[Key words] laser cladding; Co-based alloy; wear resistance; hot corrosion

[CLC number] TG 156.99 [Document code] A

1 INTRODUCTION

During the operation of gas turbines, the temperature inside the turbine can reach 900~ 1 000 ℃ or above. Usually the components in the hot-gas-path will suffer catastrophic surface attack known as hot corrosion or sulphidation. So the alloys used as the turbine component need to be high temperature oxidation resistant, high temperature fatigue resistant, wear resistant and has stable structure.

In recent years, high temperature sulphate salt corrosion behavior and electrochemical corrosion mechanisms of heat resistant Ni-base alloy, Ni-Cr alloy, and heat resistant barrier coating were studied by materials researchers[1~9]. Similar hot corrosion behavior of Co-Cr-W alloy was also systematically studied by Johnson et al[10]. However, published work on the hot corrosion behavior of laser clad heat resistant alloy coating is sparse.

This paper reports the results of laser cladding Co-based heat resistant alloy on 2Cr13 stainless steel substrate. The microstructure of the clad layer, the wear property and its hot corrosion behavior in lead sulphate fused salt crucible test are discussed.

2 EXPERIMENTAL

2.1 Materials

The substrate used was 2Cr13 stainless steel with nominal composition (mass fraction, %) of C 0.16~ 0.24, Cr 12~ 14, Si ≤0.6, Mn ≤0.6, S ≤ 0.03, P ≤0.03, and Fe balanced.

The steel slab was machined into specimen of 57 mm × 25 mm × 6 mm and 18 mm × 12 mm × 6 mm for wear and hot corrosion tests respectively.

Various commercial pure metal powders with average size of 43~ 104 μm were used for cladding. The alloy powder for laser cladding in this study was made up of Cr 14, Ni 13, W 3, Mo 4, Fe 3, Si 2.5, B 2, C 0.8, Co balanced (mass fraction, %).

2.2 Laser cladding process

The 2Cr13 stainless steel specimens were grit blasted and ultrasonic cleaned before it was powder coated by thermal spraying. The coating thickness was controlled at 0.5 mm by subsequent surface grinding. All the surfaces of the specimen for hot corrosion test were coated whereas only one surface was coated on the wear test specimen.

A continuous cross flow 2 kW CO_2 laser was used for laser cladding. The process parameters were: working power 1.5 kW, scanning speed 9 mm/s, GaSe lens 125 mm focal length, beam diameter 4 mm, overlapping at 50% interval, Ar shielding.

2.3 Analysis

The microstructure, composition and phase iden-

① [Foundation item] Project supported by the State Key Laboratory for Corrosion and Protection of Metals
[Received date] 2001- 02- 05; [Accepted date] 2001- 04- 12

tification of the laser clad layer as well as the corroded specimen and corrosion products were examined by SEM, optical microscopy and X-ray diffractometry. Vicker's hardness measurement were also carried out at the cross-sections using 200 g loading.

2.4 Wear test

Wear tests were carried out on a wear tester shown in Fig. 1. The rubber wheel with diameter of 150 mm was rotated at 240 r/min and loading on the specimen was set at 50 N. Quartz sand (SiO_2) particles of 1.0~1.2 mm in diameter were mixed with water and fed to the wheel gravitationally. The mass loss of the specimen was measured by a electronic balance with accuracy of ±0.1 mg.

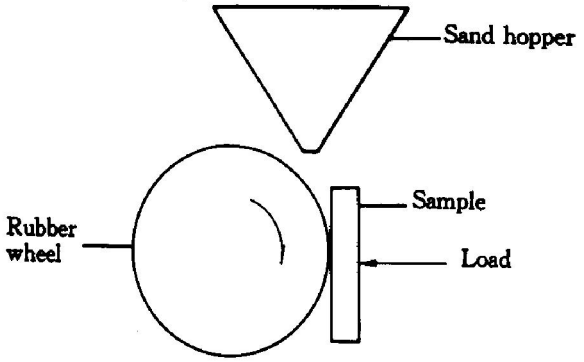

Fig. 1 Schematic diagram of wear testing

2.5 Hot corrosion

For hot corrosion crucible test, all the surfaces of each specimen were laser cladded. The clad surfaces were ground by Grade 1000 SiC paper and then polished by 1 μm diamond paste. The polished specimen was then ultrasonic cleaned and submerged in $PbSO_4$ salt inside an Al_2O_3 crucible. The crucible was then put in a furnace with constant temperature control. The range of temperature studied was 700~900 ℃. Test duration for each temperature was 24 h.

3 RESULTS AND DISCUSSION

3.1 Microstructure of clad layer

Fig. 2 shows the microstructure of the Co-base laser clad layer. The clad layer mainly has a fine dendritic structure. A 4~6 μm thick interface with single-phase structure is observed between the clad layer and the substrate. The clad layer is metallurgically bonded to the substrate. Dendrites in the clad layer grow equiaxially at the interface and along the direction of heat flow towards the centre of the clad. All dendrites have secondary arms and no columnar grain is observed. The existence of secondary dendritic arms and lack of columnar grains are important for retarding the migration of sulphur ions into the alloy during the hot corrosion process. The overlapping zone has similar dendritic structure.

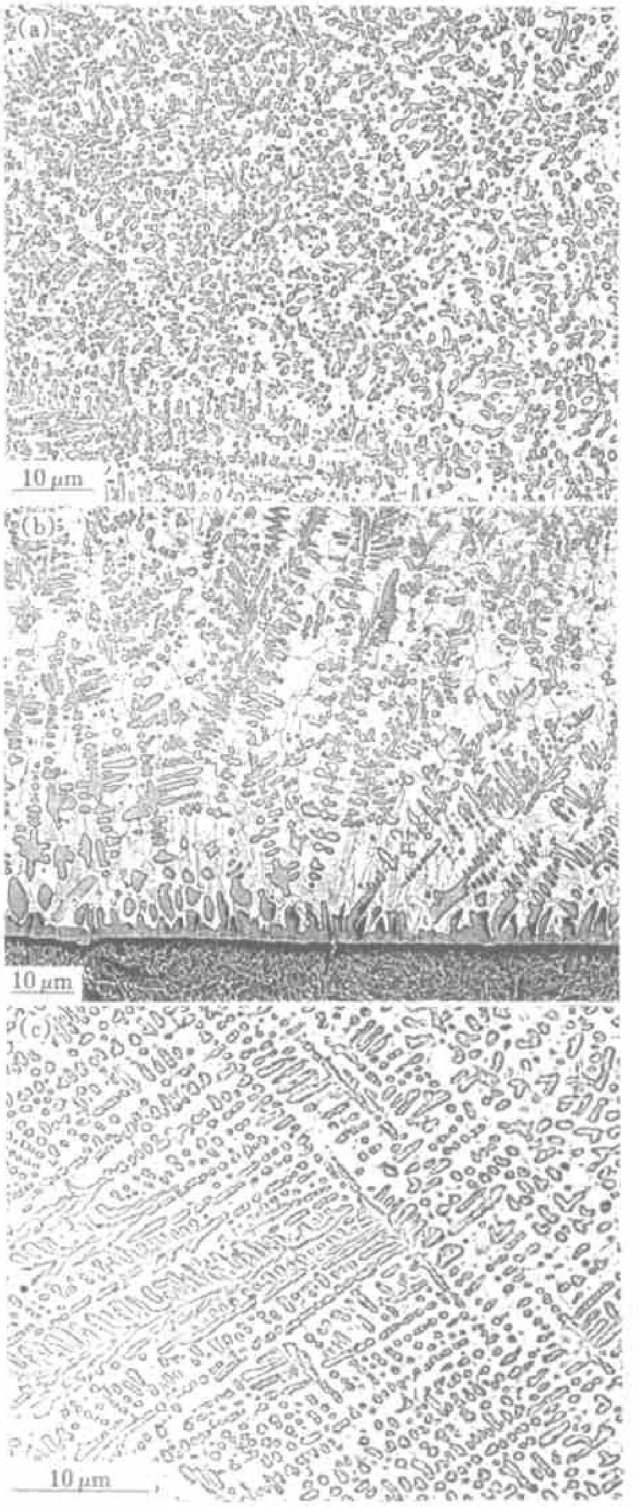

Fig. 2 Microstructure of Co-based laser clad layer
(a) —Dendritic structure of clad layer;
(b) —Interface between clad layer and substrate;
(c) —Dendritic structure of overlapping region

X-ray diffraction spectra indicates that the clad layer mainly consists of supersaturated α-Co solid solution, CrB, Co_3B, $M_{23}(CB)_6$ and μ[$(CoCr)_7W_6$] phases.

3.2 Hardness and wear properties

Fig. 3 shows the hardness value along the depth of the clad layer. The surface hardness of the clad layer is slightly higher than 1000 Hv which is 2.5

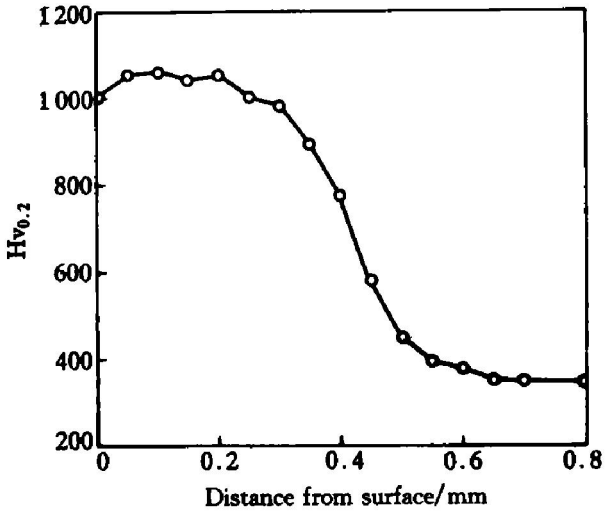

Fig. 3 Hardness profile of laser clad layer

times harder than the substrate stainless steel.

Fig. 4 shows the wear test results of the clad layer and the substrate. The clad layer has wearing resistant also 2.5 times higher than that of the substrate. This is due to the existence of various hard intermetallic phases that are bounded firmly by the cobalt matrix in the clad layer.

3.3 Hot corrosion property

Fig. 5 shows the results of the hot corrosion crucible test. For both the clad layer and the substrate, their average corrosion penetration depths increase with the temperature of the test. The hot corrosion resistance in $PbSO_4$ fused salt of the Co-base clad layer is at least 3 times higher than that of the 2Cr13 stainless steel. In addition, the lower slopes of the curves in Fig. 5 also indicate the clad layer has less temperature sensitivity compared with the stainless steel. Fig. 6 shows the hot corrosion behaviour of the Co-base clad layer in the crucible test at 900 ℃. It can be seen that there is almost a linear relationship between the corrosion depth and the time.

X-ray diffraction analysis reveals that the hot corrosion products of 2Cr13 stainless steel at 900 ℃ for 35 h are Fe_2O_3, Cr_2O_3, $FeO \cdot Cr_2O_3$, $PbCrO_4$ and FeS. As for the clad layer, the corrosion products are CoO, Cr_2O_3, $CoO \cdot Cr_2O_3$, $PbCrO_4$, Co_3S_4 and $CoO \cdot Cr_2O_3$. $PbCrO_4$ is the dominant phases. Scanning electron microscopy reveals that the main mode of corrosion is intercrystalline corrosion type for both 2Cr13 stainless steel and the Co-base clad layer, as shown in Fig. 7.

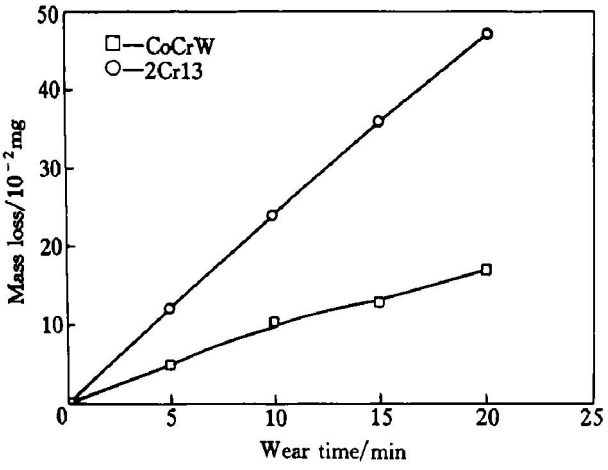

Fig. 4 Results of wear test

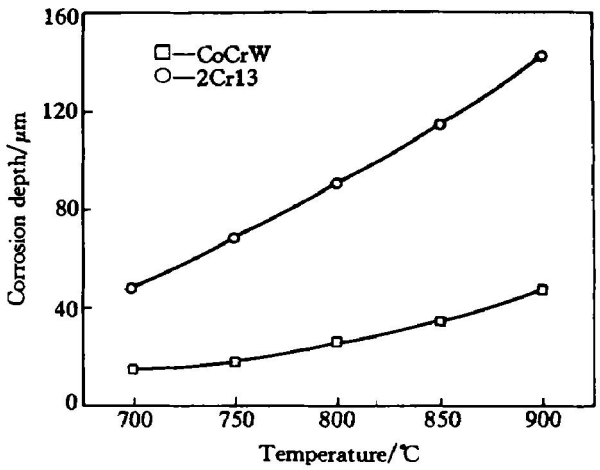

Fig. 5 Hot corrosion test result at different testing temperatures for 24 h

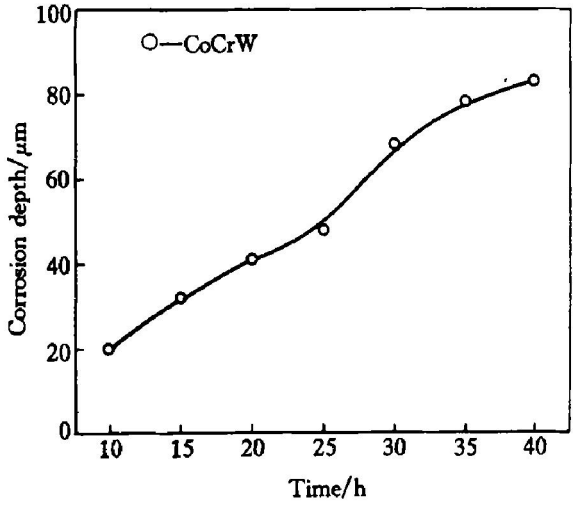

Fig. 6 Hot corrosion test result at 800 ℃ for different time

At the initial stage of the corrosion, chromium and cobalt at the outmost surface are oxidized to form a protective scale of Cr_2O_3 and CoO. Because of the existence of W and Mo in the alloy, WO_3 and MoO_3 also formed. The oxides of W and Mo have lower density and packing efficiency. Therefore it will affect the continuity of the oxide scales of the Cr and Co. This allows the diffusion of sulphur and oxygen into the fresh alloy beneath the oxide scale. At the same time, a film of sulphate salt also formed on the scale. The chemical potential gradient of oxygen and sulphur across the scale and layer of salt provides the driving force for the diffusion of oxygen and sulphur

into the alloy. The scale continues to grow and the reaction depletes the chromium at the surface. Further reaction between the Pb and Cr causes the oxide scale spall and release sulphur ion[11] at the same time. Oxygen and sulphur diffuse along the grain boundaries and form low melting point sulphides. The sulphide compounds weaken the grain boundaries and cracking occurs finally.

$$\left[Cr_2O_3 + \frac{3}{2}O_2 \quad \text{or} \quad 2CrO_3 \right] + 2O^{2-} = 2CrO_4^{2-}$$

$$\left[CrO_3 + \frac{3}{2}O_2 \quad \text{or} \quad 2CrO_3 \right] + 2SO_4^{2-} = 2CrO_4^{2-} + 2SO_3$$

$$Pb^{2+} + CrO_4^{2-} = PbCrO_4$$

$$SO_4^{2-} + 8e = S^{2-} + 4O^{2-}$$

$$Co^{2+} + S^{2-} = CoS$$

$$2Co^{3+} + 3S^{2-} = Co_2S_3$$

$$CoS + Co_2S_3 = Co_3S_4$$

Fig. 8 shows the distribution of the elements of

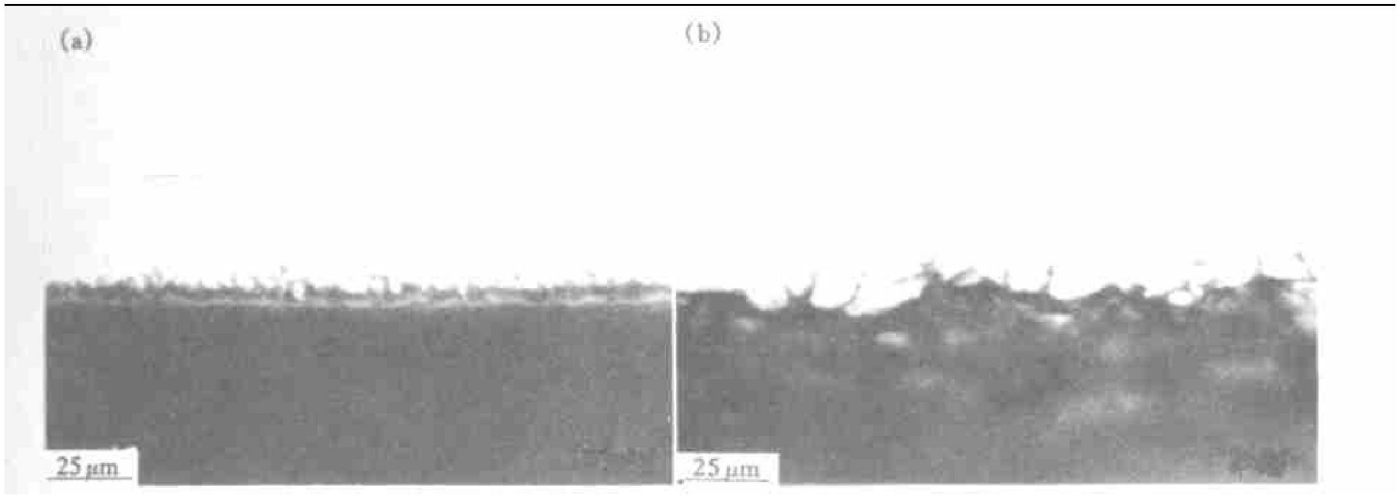

Fig. 7 Cross section of corroded specimen
(24 h, 800 ℃)

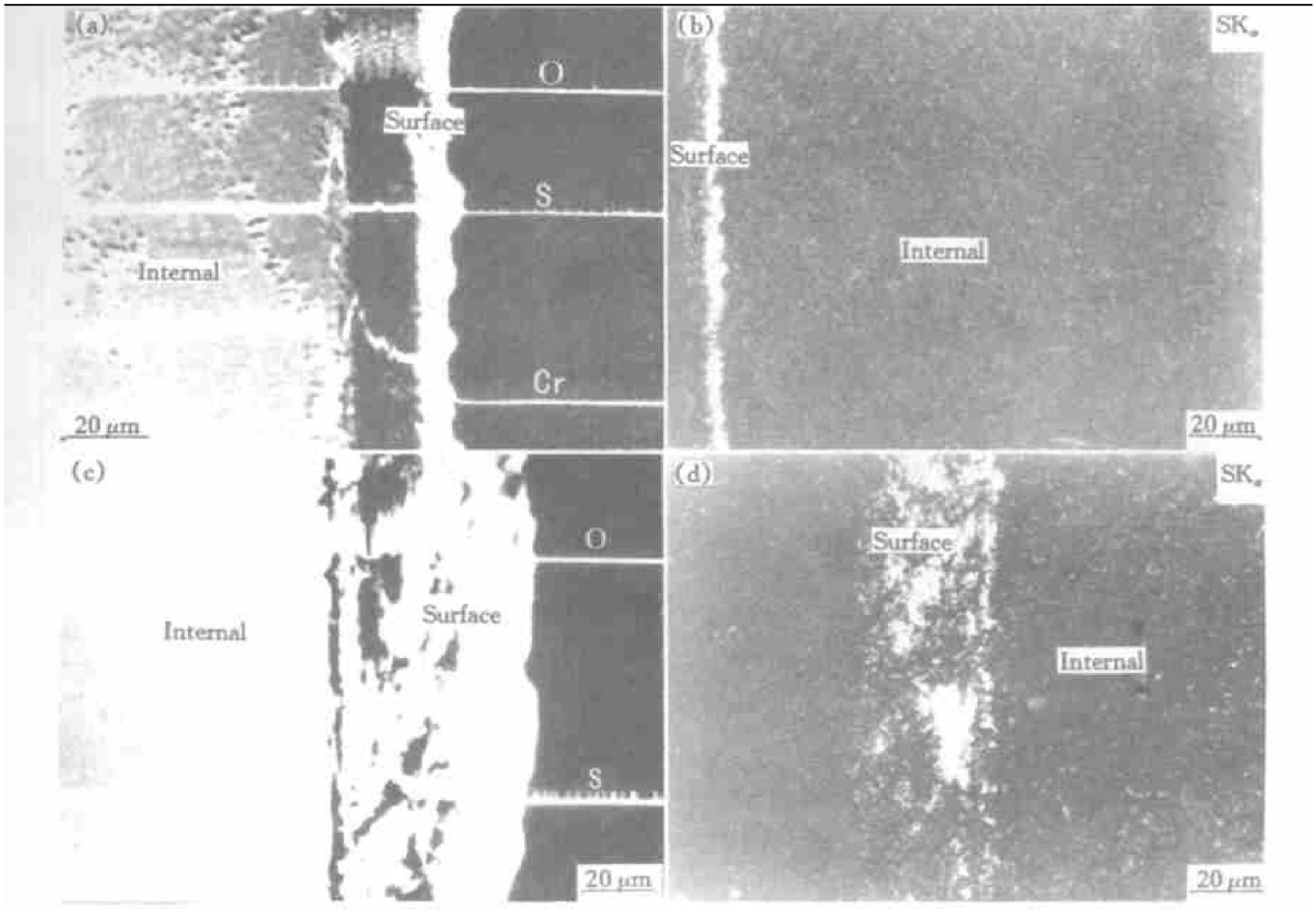

Fig. 8 Distribution of elements in samples
(a) and (b) —CoCrW laser clad layer; (c) and (d) —2Cr13 substrate

O, S and Cr from the surface after the specimen is submerged in lead sulphate at 800 ℃ for 24 h. The distribution of O and S in 2Cr13 is much wider than that in the Co-base clad layer. This indicates that the oxides of Co retard the failure of the protective oxide scale at the initial stage and also slow down the migration of sulphur into the alloy effectively. It has been confirmed that at temperature below 1 000 ℃, the diffusion rate of S into Co is lower than that of S into Ni by an order of two[12].

The existence of the fine dendritic structure of the clad layer also contributes to the improvement of the hot corrosion resistance. Migration of sulphur along the grain boundaries where various metallic carbides exist is much more difficult than that in the stainless steel with octahedral grain structure.

4 CONCLUSION

The well distributed hard intermetallic phases in the Co-base laser clad layer help to improve the hardness and wear resistance of the layer significantly. The hardness and wear resistance of the clad layer are 2.5 times higher than those of 2Cr13 stainless steel. The hot corrosion resistance of the clad layer in lead sulphate fused salt is also 3 times higher than that of the 2Cr13 stainless steel. The improvement of this property is due to the existence of Co in the clad layer that retards the failure of the protective oxide scale and slows down the migration of the sulphur along the dendritic boundaries. The fine dendritic structure also contributes to the increase of the hot corrosion resistance.

ACKNOWLEDGEMENT

Research facilities provided by the Hong Kong Polytechnic University are also appreciated.

[REFERENCES]

[1] Jong J K, Seng M C. Hot corrosion resistance of Ni and Ni-base superalloys [J]. Journal of Materials Science Letters, 1996, 15(1): 19–22.

[2] Longa-Nava Y, Zhang Y S, Rapp R A. Hot corrosion of nickel-chromium and nickel-chromium-aluminum thermal-spray coatings by sodium sulfate-sodium metavanadate salt [J]. Corrosion Science, 1996, 52(9): 680–689.

[3] Rhys-Jones T N, Swindells N. The high temperature corrosion of a commercial aluminide coating on IN738-LC and marMOO2 at 700 ℃ and 830 ℃ [J]. Corrosion Science, 1985, 25(7): 559–576.

[4] Navas G, Viloria L. Laboratory and field corrosion behavior of coatings for turbine blades [J]. Surface & Coatings Technology, 1997, 94–95(1–3): 161–167.

[5] Rapp R A, Zhang Y S. Hot Corrosion of materials-fundamental-studies [J]. Journal of Metals, 1994, 46(12): 47–55.

[6] Nishikata A, Haruyama A. Electrochemical monitoring of the corrosion of Ni, Fe, and their alloys in molten salts [J]. Corrosion, 1986, 42(10): 578–584.

[7] Otsuka N, Rapp R A. Hot corrosion of preoxidized Ni by a thin fused Na_2SO_4 film at 900 ℃ [J]. Journal of Electrochemical Society, 1990, 137(7): 46–52.

[8] Otsuka N, Rapp R A. Effects of chromate and vanadate anions on the hot corrosion of preoxidized Ni by a thin fused Na_2SO_4 film at 900 ℃ [J]. Journal of Electrochemical Society, 1990, 137(1): 53–60.

[9] CHEN Guo-feng, LOU Han-yi. Oxidation resistance of sputtered Ni-5Cr-5Al nanocrystalline coating [J]. The Chinese Journal of Nonferrous Metals, (in Chinese), 2000, 10(2): 175–178.

[10] Johnson D M, Whittle D P, Stringer J. Mechanisms of Na_2SO_4-Induced accelerated oxidation [J]. Corrosion Science, 1975, 15(1): 721–739.

[11] Sims T, Chester T. The Superalloys [M]. New York: Wiley-Interscience, 1972. 317.

[12] Landolt H. Title Numerical Data and Functional Relationships in Science and Technology [M]. New York: Springer-Verlag, 1991. 332, 204.

(Edited by YANG Bing)